


# Intraosseous Injection of Calcium Phosphate Polymer-Induced Liquid Precursor Increases Bone Density and Improves Early Implant Osseointegration in Ovariectomized Rats

Yanyan Zhou <sup>1</sup>Zihe Hu<sup>1</sup>Mingjie Ge<sup>1</sup>Wenjing Jin<sup>1</sup>Ruikang Tang<sup>2</sup>Qi Li <sup>1</sup>Weijian Xu<sup>1</sup>Jue Shi<sup>1</sup>Zhijian Xie<sup>1</sup>

<sup>1</sup>Stomatology Hospital, School of Stomatology, Zhejiang University School of Medicine, Clinical Research Center for Oral Diseases of Zhejiang Province, Key Laboratory of Oral Biomedical Research of Zhejiang Province, Cancer Center of Zhejiang University, Hangzhou, 310006, People's Republic of China; <sup>2</sup>Center for Biomaterials and Biopathways, Department of Chemistry, Zhejiang University, Hangzhou, 310027, People's Republic of China

**Purpose:** Osteoporosis, due to bone loss and structural deterioration, is a risk factor for dental implant failure, as it impedes initial stability and osseointegration. We aim to assess the effects of calcium phosphate polymer-induced liquid precursor (CaP-PILP) treatment, which significantly increases bone density and improves early implant osseointegration in ovariectomized rats.

**Methods:** In this study, CaP-PILP was synthesized and characterized through TEM, FTIR and XRD. A rat model of osteoporosis was generated by ovariectomy. CaP-PILP or hydroxyapatite (HAP, negative control) was injected into the tibia, and the resulting changes in bone quality were determined. Further, implants were installed in the treated tibias, and implantation characteristics were assessed after 4 weeks.

**Results:** The CaP-PILP group had superior bone repair. Importantly, CaP-PILP had excellent properties, similar to those of normal bone, in terms of implant osseointegration. In vivo experiment displayed that CaP-PILP group had better bone contact rate ( $65.97 \pm 3.176$ ) than HAP and OVX groups. Meanwhile, a mound of mature and continuous new bone formed. Moreover, the values of BIC and BA showed no significant difference between the CaP-PILP group and the sham group.

**Conclusion:** In summary, CaP-PILP is a promising material for application in poor-quality bones to improve implant success rates in patients with osteoporosis. This research provides new perspectives on the application of nano-apatite materials in bone repair.

**Keywords:** polymer-induced liquid precursor, calcium phosphates, nanocluster, osteoporosis, oral implant

## Introduction

The systemic disease, osteoporosis, seriously impacts the health and quality of life of older adults, and particularly of middle-aged and older women who have experienced menopause.<sup>1,2</sup> The prevalence rate of osteoporosis among Chinese women >65 years old is as high as 51.6%.<sup>3</sup> Abnormal bone metabolism caused by osteoporosis results in reduced bone mineral content, destruction of trabecular bone microstructure, inferior bone biomechanical properties and damage to bone regeneration and remodeling.<sup>4,5</sup> As it has relatively active bone metabolism, alveolar bone is the most prone to osteoporosis, which can lead to poor osseointegration of intraosseous dental implants.<sup>6,7</sup> Dental implant restoration, as the good treatment

Correspondence: Zhijian Xie; Jue Shi  
Email xzj66@zju.edu.cn; dentistsj@zju.edu.cn



for dentition defects and edentulous, cannot be applied to patients with osteoporosis, as good implant osseointegration is key to implant success.<sup>8,9</sup>

Initial implant stability is a major determinant of implant integration.<sup>10</sup> Numerous basic and clinical studies have confirmed that initial implant stability is reduced in osteoporotic bone, which prolongs the healing time of implant bone and increases the risk of implant loosening.<sup>11,12</sup> Achievement of initial stability at an early stage of implantation is a major concern for dentists working with osteoporosis patients. Various methods to achieve stability have been attempted, including implant surface modifications (such as roughening or chemical modification of surfaces),<sup>13–15</sup> surgical operations (such as the split-crest technique),<sup>16,17</sup> and drug therapies (such as estrogen and bisphosphonates).<sup>18–20</sup> Nevertheless, implant surface modification does not improve bone formation or rebuild bone balance and remains far from clinical application.<sup>21</sup> Surgical trauma can easily lead to cortical fractures of the fragile alveolar bone, increasing the risk of implant failure.<sup>22</sup> In addition, traditional drugs can have serious adverse effects, such as osteonecrosis of the jaw, subtrochanteric fractures, eczema, cellulitis, and osteosarcoma.<sup>23</sup> Therefore, exploring effective and appropriate methods to improve osseointegration for orthopedic applications in patients with osteoporosis is challenging.

Bone is an organic-inorganic composite multilevel material, with complex structure and function, which principally comprises type I collagen and calcium phosphate crystals.<sup>24,25</sup> Micromechanics data indicate the importance of mineralized collagen fibers, which provide bone strength characteristics.<sup>26,27</sup> In mineralization, the crystallographic c-axis of apatite aligns almost parallel to the collagen fiber direction via an apatite crystallization on the collagen template, and the stronger direction of apatite and collagen co-aligns in one direction, which makes the bone stiff and tough in the collagen/apatite-oriented direction.<sup>28</sup> Hence, mineralized fibers are clearly of great significance to the biological and mechanical properties of bone.

Polymer-induced liquid-precursor (PILP) is a liquid-phase amorphous mineral precursor stabilized by charged polymeric additives.<sup>29,30</sup> In nature, this amorphous precursor phase plays key roles in the formation process of zebrafish fin, and rat skull and long bones.<sup>33</sup> Recently, it has been suggested that calcium phosphate-PILP can penetrate collagen fibers and occupy the internal nanoscale space, promote intrafibrillar mineralization through the

formation of co-oriented arrays of lamellar HAP crystal within the fibrils,<sup>31,32</sup> and eventually form hierarchical ordered bone structure. These findings deepen our understanding of biomineralization and provided inspiration for the development of biomimetic materials, with bone conduction and osteoinduction abilities.<sup>34</sup> Yang et al. synthesized a biodegradable mesoporous carrier to transport ACP mineralization precursors, which were available to newly deposited collagen fibrils in injured sites for collagen biomineralization and bone regeneration.<sup>35</sup> Further, Zhao et al. developed a CMCh-ACP injectable and bioprintable hydrogel, which had excellent osteoinduction effects and could significantly improve the efficiency and maturity of bone formation in vivo.<sup>36</sup> In previous experiments, our group utilized PAA to prepare homogeneously distributed and ultra-small (approximately 1 nm) CaP-PILP,<sup>37,38</sup> which could efficiently increase bone mass, bone density and mechanical properties in an osteoporotic rat model through intrafibrillar mineralization.<sup>37</sup>

Based on previous studies, here we confirmed the considerable advantages of CaP-PILP for repairing osteoporosis and assessed the potential of CaP-PILP to improve implant osseointegration under osteoporotic conditions as shown in Figure 1. First, a female ovariectomized (OVX) rat model was established to simulate osteoporosis in middle-aged and older postmenopausal women, which was a well-accepted animal model for osteoporosis.<sup>5,19</sup> Then, CaP-PILP was injected into the tibias of osteoporotic rats to improve bone quality. Further, implants were installed, and interfacial bone healing assessed, alongside histological observation to evaluate improvements in osteoporosis osseointegration.

## Materials and Methods

### Synthesis of CaP-PILP

CaP-PILP was prepared with reference to the method developed in the laboratory of Professor Tang.<sup>37</sup> CaCl<sub>2</sub>, Na<sub>2</sub>HPO<sub>4</sub>, and poly acrylic acid (PAA) (Mw, 450,000 Da) were purchased from Sigma Aldrich (Beijing, China). Polyaspartic acid (PASP) (Mw = 9000–11000 Da) was from Ai-ke Chemicals (Chengdu, China). NaOH was from Sinopharm Chemical Reagent Co, Ltd (Shanghai, China). First, Solution A was prepared by mixing 4.3 g PAA, 2.15 g PASP, and 0.7284 g Na<sub>2</sub>HPO<sub>4</sub> in 50 mL deionized water and agitating by magnetic stirring overnight. Then, 2 mL of Solution A was added slowly, dropwise into a transparent solution containing a mixture of

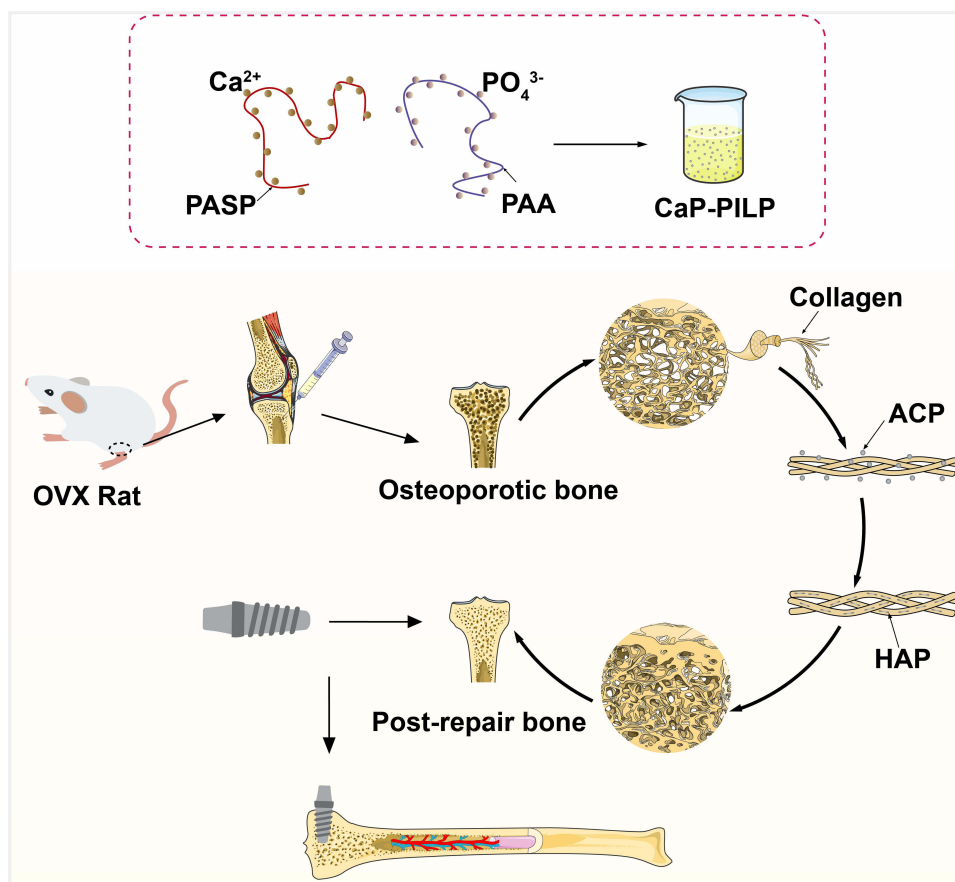


**Figure 1** Schematic diagram: the early effects of CaP-PILP treatment of implant osseointegration in regenerated osteoporotic bone in vivo: The synthesis and injection of CaP-PILP; The Repair pattern of CaP-PILP in osteoporotic bone; The installation of implants in rat's tibial. The CaP-PILP increases bone density and promotes the formation of the new bone around Ti implants.

2 mL 0.1 M  $\text{CaCl}_2$  and 0.15 mL PASP (0.3 g/mL), under ambient conditions, and the pH value adjusted to 7.4 using NaOH.

### Characterization of CaP-PILP

To determine the characteristics of CaP-PILP, a field emission transmission electron microscope (TEM, 2100F, Japan) was used to observe the morphology of ACP in the material and an EDS system was used to evaluate the content of Ca, P. Before test, samples were dissolved in ethanol and diluted 100 $\times$ , then dropped on Nickel mesh support film (T10023N, Beijing XXBR Technology Co., Ltd, China), absorbed the excess liquid, and dried it naturally. For other tests, after the CaP-PLIP was pre-frozen at  $-80^\circ\text{C}$  for 2 h, and put it into a vacuum freeze dryer for 24 h. X-ray diffraction (XRD, Bruker D8 Advance, Bruker, Germany) was used to determine whether there was an amorphous phase in freeze-dried samples. Briefly, samples were lyophilized and ground into fine powder, mixed with KBr, and pelletized in a dish, then wave frequency

analyzed in the range 500–4000  $\text{cm}^{-1}$ , and the content of inorganic matter detected by thermogravimetric analysis (TGA; TGAQ-500, TA instrument). The heating rate was  $10^\circ\text{C}/\text{min}$  in air, with a range of room temperature to  $600^\circ\text{C}$ .

### Establishment of an Osteoporosis Model

All animal experiments were carried out at Zhejiang Chinese Medical University Laboratory Animal Research Center, according to guidelines approved by the Laboratory Animal Management and Ethics Committee (IACUC-20180502-03). Female Sprague Dawley rats (12 weeks old) were used after acclimatization to their new environment for 1 week. After 12 h for fasting, 56 SD rats were assigned randomly to two groups: OVX group (40), sham operation (sham) group (16). Each rat was anesthetized with 3% pentobarbital (1.5 mL/kg body weight). Then, ovariectomy<sup>39</sup> was carried out by making a small incision on the belly line of each rat to remove both ovaries, and the incision closed layer by suture. For sham-operated rats, incisions were made and an

equivalent amount of fat removed instead of the ovaries. 12 weeks after surgery, four rats were randomly selected from sham and OVX groups. Microcomputed tomography (micro-CT) was used to observe and analyze bone microstructure changes to confirm that the osteoporosis model was successfully established.

## CaP-PILP Injection

Rats that had undergone ovariectomy or a sham operation were divided into four groups: (1) sham group, (2) OVX group, (3) ovariectomy and a percutaneously minimally invasive injection of CaP-PILP into the osteoporotic tibia (CaP-PILP group), and (4) ovariectomy and a percutaneously minimally invasive injection of HAP ( $[\text{Ca}_5(\text{OH})(\text{PO}_4)_3]_x$ , <100nm particle size, Aladdin, China) into the osteoporotic tibia (HAP group), each with 12 rats. Treatments were initiated in the 12th week after ovariectomy. Briefly, rats were anesthetized and 50  $\mu\text{L}$  of prepared CaP-PILP or HAP minimally invasively was injected into the osteoporotic tibia. Subsequently, 4, 8, and 12 weeks after drug injection, 4 rats in each group were randomly selected for evaluation. In vivo osteoporotic bone recovery ability was evaluated using micro-CT to determine the appropriate time for implant installment.

## Implant Installation

Twenty rats were divided into four groups. Based on the above method, the model was established. After the drug was injected for an appropriate time, implants were implanted. Screw-shaped titanium implants (dimensions: diameter, 1.5 mm; length, 4 mm) were obtained from Guangci MD Co (Ningbo, China). Two screws were inserted into the right and left tibial metaphysis of animals. Briefly, after rats were anesthetized and shaved, a 5 mm incision was made on the internal side of knee joints, and soft tissue was pushed aside via periosteum dissection to expose the surgical area. A 1.3-mm diameter drill was used to prepare the surgical site. The operation area was irrigated with physiological saline to lower the local temperature and reduce tissue damage. Screws were directly rotated into the hole using the self-tapping technique. Subsequently, the soft tissue was sutured back layered. Following surgery, rats were administered 50,000 U penicillin G benzathine intramuscularly daily for three days.

## Micro-CT Evaluation of Bone Microstructure

Four weeks after surgery, rats were euthanized in 100%  $\text{CO}_2$ , and tibias harvested and fixed in 4% paraformaldehyde for 24 h. A micro-CT system (milabs U-CT, the Netherlands) was used to assess osseointegration between the screws and the surrounding bone. The measurement conditions were as follows: 90 kV, 0.2 mA, voxel size 20  $\mu\text{m}$ , and exposure time 300 ms. A full 3D reconstruction of the implant was generated using software (Imalytics Preclinical), with a radius of 3 mm around the implant identified as defined region of interest (ROI). According to the manufacturer's technical instructions, related morphometric parameters, including bone volume/total volume (BV/TV, %), bone mineral density (BMD, units), and trabecular separation (Tb.Sp, cm), were analyzed.

## Fluorescence Labeling of Bone Specimens and Histologic Analysis

To evaluate the new bone around the implant, alizarin red (30 mg/kg; Sigma) and fluorochrome calcein (20 mg/kg; Sigma) were administered to each animal intramuscularly 2 and 3 weeks after surgery, respectively, as double-fluorescent labeling.<sup>40</sup> Hard tissue slices were generated to evaluate the bone-implant interface and calculate bone implant contact (BIC). Briefly, samples were dehydrated in a graded series of ethanol (70%, 90%, and 100%), embedded in resin, photopolymerized, and the tissue was cut by a tungsten steel knife on the slicer, then ground to an ideal position (approximately 10  $\mu\text{m}$  thickness along the long axis of the implant) on the grinding machine. Calcium precipitation labeled by alizarin red (old bone) and calcein green (new bone) fluorochromes were observed by fluorescence microscopy. Images were obtained separately, reconstructed, and the overlap of fluorochrome areas used to quantify the mineral apposition rate (MAR).<sup>41</sup> Subsequently, sections were stained with acid fuchsin-methylene blue, and light microscopy was used to capture the images. The area around the implant thread was chosen as a ROI to calculate bone-to-implant contact (BIC%) and neo-formed bone area (NBA) using Image J software.

## Absorption of Ca, P

150  $\mu\text{L}$  of collagen solution (Gibco, the US) was dropped into a clean dish, placed for 4 h in the ratio of ammonia to deionized water 1:1 to form collagen gel,

then soaked in deionized water for 30 min. Drop 50ul prepared CaP-PILP onto the surface of collagen gel, and add 450 $\mu$ l deionized water for sustained release. A total of 21 groups of samples were prepared, and 3 groups were randomly selected for testing every day. Before the test, 200 ul released liquid was added to 8 mL 5% dilute nitric acid. The release concentration of Ca and P was detected by ICP-MS (Agilent 7800, USA). The amount of Ca and P deposition was calculated by the total amount of Ca and P added to the material, and the mineralization rate in vitro was evaluated.

## Statistical Analysis

Data are presented as the mean $\pm$ standard deviation. The data were tested for normality using the Shapiro–Wilk test in SPSS software. If followed by a normal distribution, the statistical differences of data were assessed by Student's *t* test and one-way analysis of variance (ANOVA), followed by Tukey's test;  $P < 0.05$  was considered statistically significant. If not, non-parametric statistical tests were used.

## Results

### Characterization of CaP-PILP

As shown in Figure 2A and B, CaP-PILP was a yellow, transparent, viscous, and injectable liquid. TEM analysis indicated that CaP-PILP comprised amorphous nanoclusters of approximately 1 nm (Figure 2C). XRD and FTIR further confirmed that amorphous calcium phosphate was successfully prepared (Figure 2D and E). The stretching vibration and bending vibration peak of  $\text{PO}_4^{3-}$  were at  $542\text{ cm}^{-1}$  and  $1060\text{ cm}^{-1}$ , respectively. The broad and strong absorption peak at  $3424\text{ cm}^{-1}$  was represented for the O-H stretching vibration absorption of carboxylic acid, and the stretching vibration of C=O was observed at  $1597\text{ cm}^{-1}$ . And, the peak at  $1409\text{ cm}^{-1}$  and  $1313\text{ cm}^{-1}$  resulted from the absorption peaks of O-H in-plane bending vibration and C-O stretching vibration of PAA. XRD revealed a broad peak at  $2\theta = 30^\circ$ , this wide peak showed that the material being examined did not contain any crystals. TGA curves showed that the solidified material comprised 27 wt% mineral, 31 wt% organics, and 42 wt% water (Figure 2F). The EDS result of CaP-PILP showed the content of Ca and P in Figure S1. As shown in

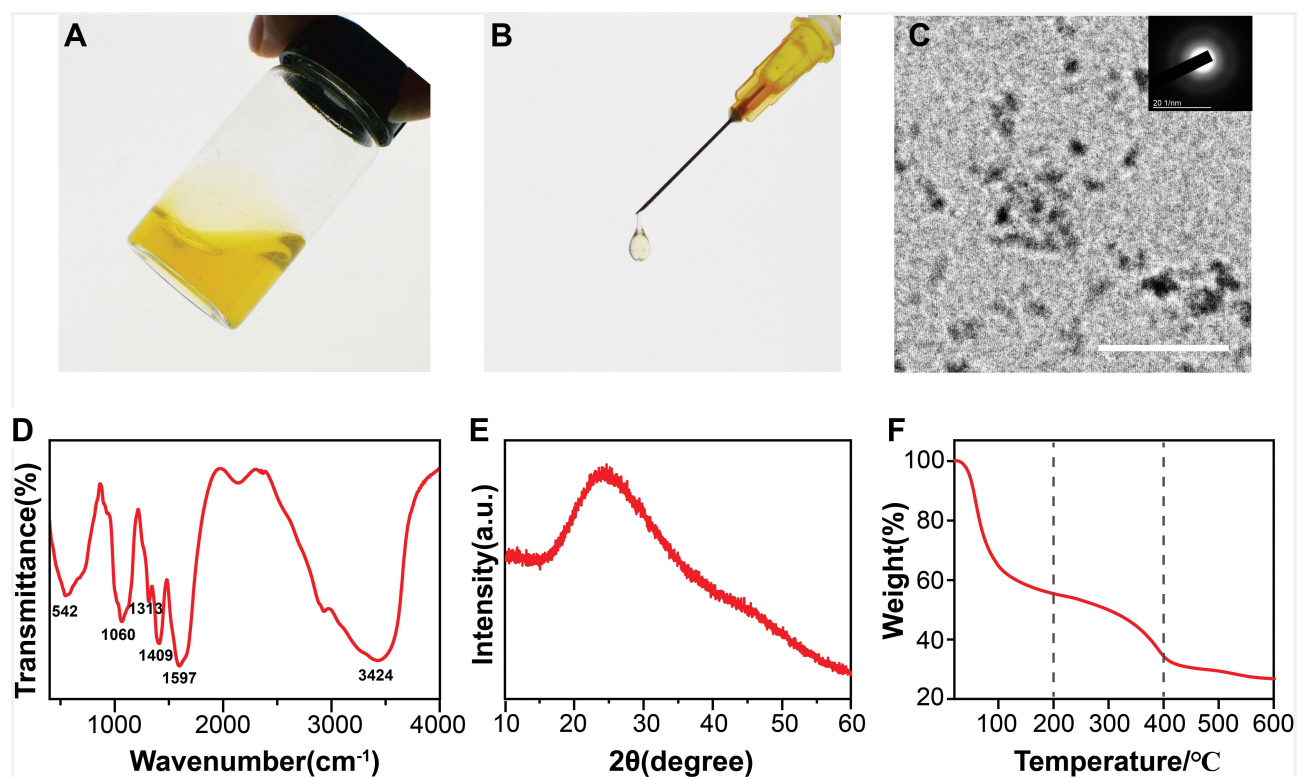


**Figure 2** Preparation and characterization of CaP-PILP. (A) Photograph of CaP-PILP; a yellow, transparent and viscous fluid. (B) Photograph of CaP-PILP injection using a 1-mL syringe, showing that the material is flowing and injectable. (C) TEM images of CaP-PILP, indicating that the size of ACP is approximately 1 nm. The SAED shows that the clusters are amorphous. (scale bar, 10 nm). (D) FTIR spectrum, (E) pXRD spectrum, and (F) TGA curve of CaP-PILP.

[Figure S2](#), the absorption of Ca and P in the collagen gel was a slow process before 4 days and tended to be stable.

## CaP-PILP Improved Periprosthetic Bone Mass in a Rat Model of Osteoporosis

OVX rats were the most commonly used animal model for postmenopausal osteoporosis. Here, results demonstrated that an osteoporosis rat model was successfully established ([Figure S3](#), 4). The surgical procedures of CaP-PILP injection and implant insertion in rats are shown in [Figure 3](#).

Rats were harvested after drug injection at 4, 8, and 12 weeks and micro-CT was used to evaluate bone repair in each group ([Figure 4A](#)). BV/TV (%), and BMD (units), Tb.Sp (cm) were analyzed using micro-CT software and the results presented in graphical form ([Figure 4B–D](#)). After 4 weeks, there was a small amount of bone formation in the CaP-PILP group, which did not differ significantly from that in HAP and OVX groups. Micro-CT analysis revealed that BV/TV; BMD and Tb.Sp in sham groups had a significant difference ( $p < 0.01$ ) than in the other three groups ([Figure 4B–D](#)). After 8 weeks, bone mass increased significantly in the CaP-PILP group. Although the data in CaP-PILP group were lower than that in the sham group (BV/TV:

$p < 0.01$ ; BMD:  $p < 0.05$  and Tb.Sp:  $p < 0.01$ ), a significant difference was found between OVX group and CaP-PILP group. Micro-CT analysis revealed that BV/TV in CaP-PILP group ( $0.31 \pm 0.122$ ) was significantly higher ( $p < 0.01$ ) than that in OVX group ( $0.14 \pm 0.021$ ). Likewise, the value of BMD in CaP-PILP group ( $1.46 \pm 0.42 \times 10^3$ ) was significantly elevated than those of OVX ( $0.69 \pm 0.96 \times 10^3$ ) and HAP groups ( $0.82 \pm 0.16 \times 10^3$ ) ( $p < 0.01$ ). CaP-PILP group tended to perform better in BMD. For Tb.Sp, CaP-PILP group appeared to decrease ( $0.0386 \pm 0.0158$ ), while HAP group ( $0.0616 \pm 0.0038$ ) was abnormally increased, and there was a distinct difference between the two groups ( $p < 0.01$ ). At 12 weeks, bone repair in CaP-PILP group showed a slower growth trend compared with 8 weeks. While rats in both the HAP and OVX groups showed better bone improvement, they were still lower than CaP-PILP group. Interestingly, no significant difference was found between the CaP-PILP group and the sham group.

Overall, CaP-PILP significantly promoted the bone repairment in osteoporosis rats, and the best time to repair osteoporosis was 8 weeks after injection, when new bone formation increased significantly to the maximum value and there was no significant increase later.



**Figure 3** (A) The surgical procedures of the minimally invasive injection of CaP-PILP into tibia. (B) The implant surgery procedures in rats, including skin incision, implantation hole, implant insertion, layered sutures.

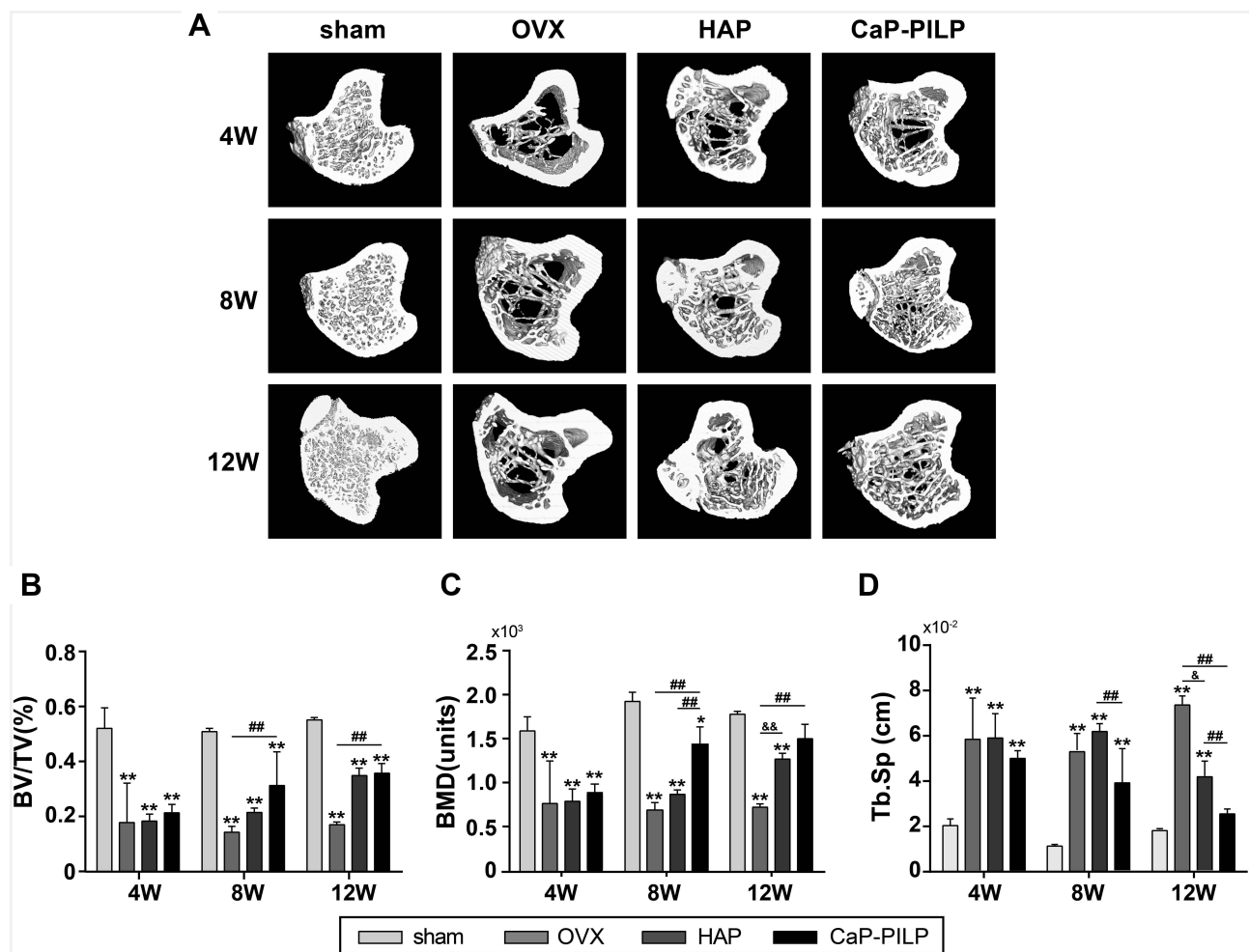


**Figure 4** Micro-CT images and analysis in the following groups of rats: sham, OVX, HAP and CaP-PILP group after 4, 8, and 12 weeks. **(A)** Reconstructed Micro-CT images of tibia transverse. Quantitative analysis of micro-CT data: **(B)** Percent bone volume (BV/TV). **(C)** Bone mineral density (BMD). **(D)** Trabecular separation (Tb.Sp). Data were expressed as mean  $\pm$  SD ( $n = 5$ ); \* $P < 0.05$ ; \*\*, ###, or &&  $P < 0.01$  (ANOVA), \*Represents comparison with sham group, #Represents comparison with CaP-PILP group and &Represents the comparison between HAP group and OVX group.

### CaP-PILP Increased Implant Osseointegration in Osteoporosis Rats Microtomographic Analysis of Implants

Micro-CT analysis confirmed that CaP-PILP could improve bone quality and enhance implant osseointegration in osteoporotic rats. Three-dimensional images reconstructed by micro-CT (Figure 5A) clearly illustrated new bone formation around the implants. The highest level of newly formed bone was detected in the sham and CaP-PILP groups, followed by the HAP and OVX groups. Quantitative analysis of micro-CT data, including calculation of BV/TV (%), BMD (units), and Tb.Sp (cm) presented as a bar graph. CaP-PILP injection to OVX rats could enhance the BV/TV level ( $75.60 \pm 1.57$ ) even though the level was still lower than that in the sham group ( $77.98 \pm 2.18$ ), but there was not significantly

different (Figure 5B). However, BV/TV levels in HAP and OVX groups were significantly lower than the other two groups and had statistical differences. There was no significant difference in BMD among sham, HAP and CaP-PILP group (Figure 5C). CaP-PILP group ( $0.036 \pm 0.008$ ) tended to improve the trabecular bone microstructure, resulting in a similar level to the sham group ( $0.028 \pm 0.008$ ) in Tb.Sp. Conversely, HAP group showed an abnormal increased level ( $0.048 \pm 0.008$ ) and was significant different with sham ( $p < 0.01$ ) and CaP-PILP group ( $p < 0.05$ ) (Figure 5D).

### Histological and Histomorphometric Analysis

Bone turnover around the implants is shown in Figure 6A. Alizarin (red color) and calcein (green color) were used to stain calcium precipitation. According to the order of administration, the presence of old bone was illustrated

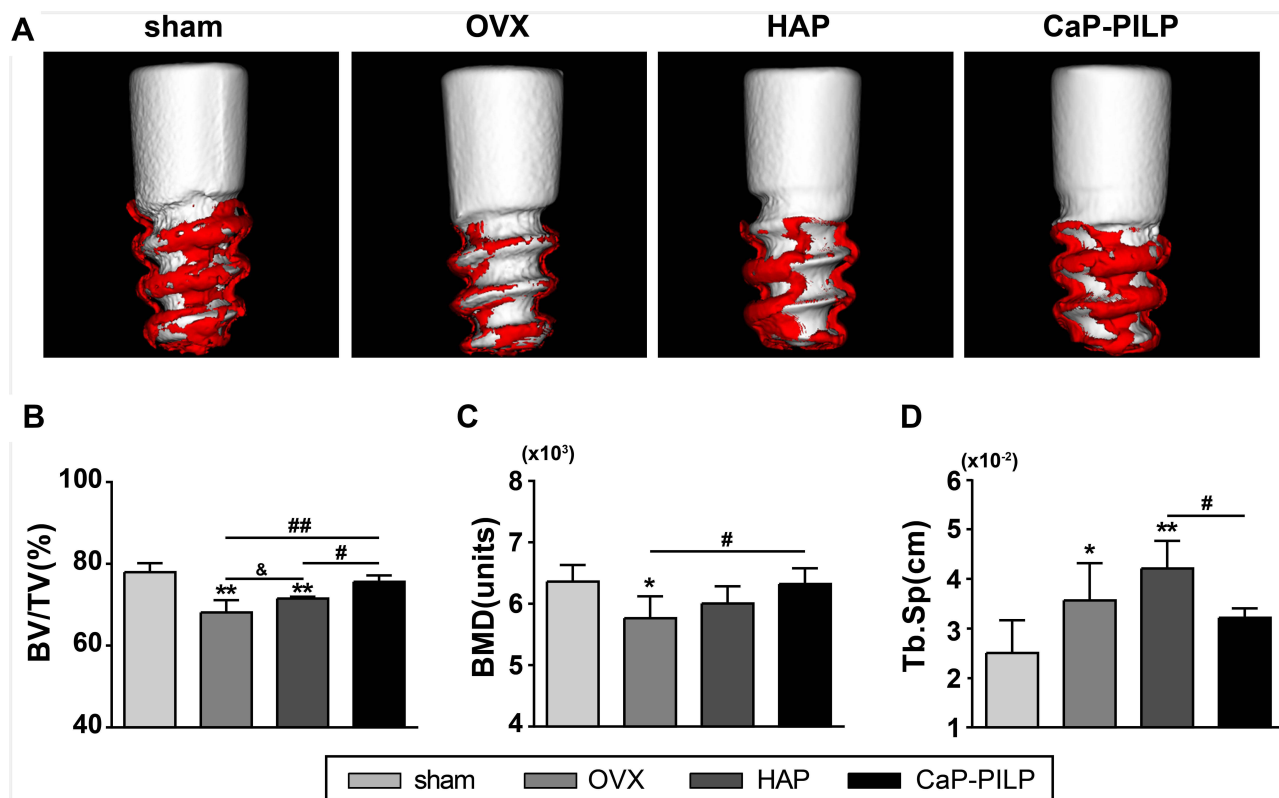


**Figure 5** Assessment of implant osseointegration in the following groups of rats: sham, OVX, HAP and CaP-PILP group, after implantation in vivo for 4 weeks. **(A)** Representative 3D reconstruction images of peri-implant region, showing the new bone formation. Bone parameters of ROI around the implant: **(B)** BV/TV. **(C)** BMD. **(D)** Tb.Sp. Data were expressed as mean  $\pm$  SD (n = 5); \*, # or &, P < 0.05; \*\* or ## P < 0.01 (ANOVA), \*Represents comparison with sham group, #Represents comparison with CaP-PILP group and &Represents the comparison between HAP group and OVX group.

by red fluorescent areas, while new bone was indicated by green areas. There was no significant difference in area of red fluorescence among the four groups, while the comparisons of levels of green fluorescence area showed that the sham group > CaP-PILP group > HAP group > OVX group (Figure 6C). Further, levels in the CaP-PILP ( $12.34 \pm 1.267$ ) and sham groups ( $15.81 \pm 1.549$ ) did not differ significantly, while there was a significant difference between the sham group and the other two groups. MAR, a dynamic histomorphometric parameter indicating the thickness of newly formed mineralized bones in unit time, was used to quantify the formation of new bones. As shown in Figure 6D, the CaP-PILP group had the highest bone turnover ( $0.93 \pm 0.064$ ), which was significantly higher than those in the OVX ( $0.53 \pm 0.077$ ,  $p < 0.01$ ) and HAP groups ( $0.59 \pm 0.072$ ,  $p < 0.01$ ), but still lower than sham group ( $1.24 \pm 0.129$ ,  $p < 0.05$ ). Figure 6B shows that in the sham group, approximately 80% surface around the implant was covered with deposits of calcified bone matrix, and the new bone was in close contact with the implant with no clear gaps. CaP-PILP group also had good

bone contact (BIC:  $65.97 \pm 3.176$ , Figure 6E) and there was a mound of mature, continuous, and compact new bone formation (BA:  $25.47 \pm 1.575$ , Figure 6F). Moreover, BIC and BA values in the CaP-PILP group did not differ significantly from those in the sham group. In the OVX group, a small amount of red-stained new bone was detected around the implant without direct contact. There was slight more formation of new bone in the HAP group than the OVX group, and some new bone made direct contact with the implant.

## Discussion

Postmenopausal osteoporosis is a common human metabolic disease.<sup>42,43</sup> Lack of estrogen leads to bone metabolism disorders and bone mass loss.<sup>44</sup> Furthermore, the microstructure and physicochemical composition of bone matrix are affected; the quality of mineralized collagen fibers is reduced, resulting in a significant decrease in the bone calcium-to-phosphorus ratio, which is considered an indicator of bone matrix quality.<sup>45,46</sup> More importantly, bone mineralisation may be altered due to changes in ion



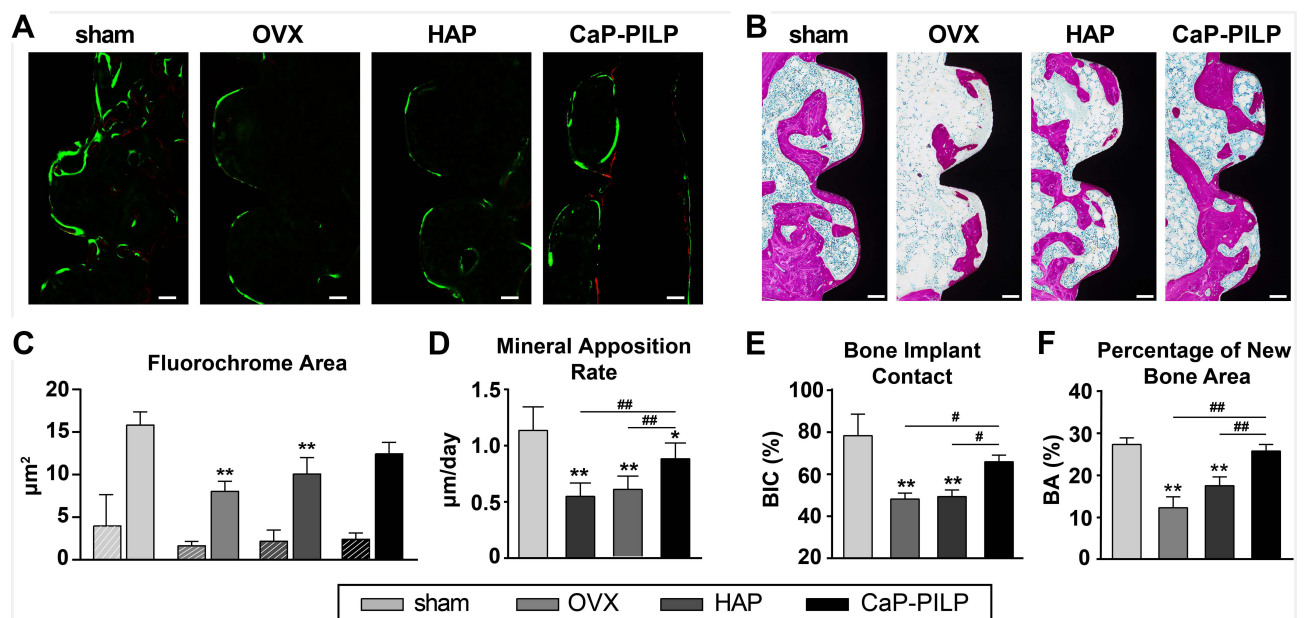


**Figure 6** Histological and histomorphometric analysis of the following groups of rats: sham, OVX, HAP and CaP-PILP group, after implantation in vivo for 4 weeks. **(A)** Double fluorescence labeling images. Red alizarin color: old bone; green calcein color: new bone (scale bar, 100 µm). **(B)** Histological sections stained with Acid fuchsin-methylene blue. Quantitative analysis: **(C)** Fluorochrome area. **(D)** Mineral apposition rate. **(E)** Bone implant contact. **(F)** Percentage of new bone area. Data were expressed as the mean ± SD (n = 5); \*or <sup>#</sup>P < 0.05; \*\*or <sup>##</sup>, P < 0.01 (ANOVA); \*Represents comparison with sham group, <sup>#</sup>Represents comparison with CaP-PILP group.

exchange and mineral chemistry.<sup>5,47,48</sup> This altered crystallization can affect the hardness, solubility, and fragility (among other parameters), of bone, and thus the overall quality of bone tissue.<sup>49,50</sup> At present, most therapeutic agents for osteoporosis are antiresorptive medications, including bisphosphonates (BPs),<sup>51</sup> parathyroid hormone,<sup>52</sup> and raloxifene,<sup>53</sup> among others. These drugs are clearly successful in combating bone loss; however, they make no contribution to induction of bone formation,<sup>54</sup> while bone mass and bone quality are important factors that determine the success of dental implants.<sup>55,56</sup> Thus, alternative, more effective methods of osteoporosis treatment are needed.

In this study, CaP-PILP was synthesized for injection to repair osteoporosis, facilitating implant osseointegration. CaP-PILP was composed of uniformly distributed amorphous calcium phosphate (ACP) clusters, with a high concentration of ultra-small size particles (1 nm). CaP-PILP had good injectability, allowing the use of minimally invasive injection methods to deliver ACP to the tibia.<sup>37</sup> ACP serves as a transient precursor to HAP, which can be deposited in intrafibrillar regions by direct or extra-fibrous particle delivery, and then converted into HAP aligned with the orientation of collagen fibers;<sup>57,58</sup> this effect may be important for bone repair. Biocomposites containing ACP have been used to treat caries, as well as

for remineralization, bone repair, and in other applications;<sup>34,44</sup> however, preparation of ACP is extremely difficult because of its polymorphism and transience, which limits its application in biomedicine.<sup>59</sup> High concentration ACP tends to exist in a more stable crystal form, while low concentrations are insufficient to provide sufficient calcium and phosphorus ions.<sup>60</sup> Many studies have attempted to use high-concentration polymers to encapsulate and stabilize sufficient ACP but have focused solely on crystallinity and ignored the effects of ultra-small particle size.<sup>29,37,61</sup> Collagen fibrils are twisted collagen triple-helix molecules that contain only approximately 1.8–4 nm-sized tortuous subchannels.<sup>37</sup> Such an exceptional structure is inaccessible to most ACP polymers by direct precipitation, which limits the performance of ACP. Here, two negatively charged polymers, PAA and PASP, were used to synergistically prepare CaP-PILP and ensure the stability of ultra-small particle size ACP. Previous studies have shown that ultra-small particle size ACP can easily pass through the collagen interstitial area, orient to the collagen matrix, and then crystallize in the fibrils to form mineralized collagen fibrils. Further, the core mechanism underlying CaP biological activity is partial dissolution and release of ionic products in the body, with size and crystallinity important factors that determine the absorption rate.<sup>31,33,58</sup> Ultra-small particle size and

amorphous ACP provide particular advantages for degradation. As a reservoir of calcium and phosphorus, ACP partially dissolves to increase local ion concentrations, affects the bone marrow microenvironment, participates in cell responses, and thereby regulates the rate of bone formation, and enhances the potential for this process to occur.<sup>47,62,63</sup>

After CaP-PILP was injected, high concentration and ultra-small particle size ACP clusters were quickly dispersed throughout the bone marrow cavity. When an initial inflammatory response occurred, the osteoclasts were activated, promoting the degradation and absorption of materials.<sup>62,64</sup> This may explain why there was almost no difference in the repair effect at 4 weeks. With continuous degradation of CaP-PILP, ACP restricted by the polymer was exposed, quickly recognized and penetrated the collagen fibers, located nucleation sites, and aggregated into an ordered crystal phase along the C axis through directional attachment, giving the damaged collagen fibers corresponding biomechanical properties.<sup>30,47</sup> Furthermore, the high content of phosphorylated anion side chains in the stabilizer, PASP, participated in the biomineralization process by contributing to induction of collagen mineralization.<sup>25</sup> Additionally, some ACP degraded, which increased the concentration of calcium and phosphorus ions in the environment. Osteoblasts sensed the partially dissolved and disordered bone minerals, leading to regulation and initiation of osteogenic signals, and enhanced differentiation and extracellular matrix generation.<sup>47,65,66</sup> Subsequently, the local supersaturated ions recrystallized, deposited, and induced natural biomineralization of newly formed tissues,<sup>24,67</sup> and then bone regeneration accelerated. Our results reflected this sharp change; at 8 weeks, BV/TV values were significantly increased, and BMD recovery was excellent; although the mean value was slightly lower than that in the sham group, the difference was not significant, and it was significantly better than those of the HAP and OVX groups. Tb.Sp also showed a significant downward trend, indicating that osteoporosis had been relieved. At 12 weeks, bone repair improved further, but the difference was not significant, possibly because calcium and phosphorus ions had become depleted without additional supplementation.

Conversely, the HAP group did not show significant improvement until 12 weeks, and was still not comparable with the other groups. Although it has the same chemical composition as ACP, HAP comprises highly stable crystals with strong anisotropy in its crystal lattice, and usually

takes the form of elongated needles or plates.<sup>31,68</sup> Although HAP is nano-sized, it has a lower ability to induce collagen mineralization than ACP.<sup>25,30</sup> Due to the low rate of HAP absorption and degradation, osteoclasts become more active and cause more bone resorption when they are exposed to HAP.<sup>32,66,69</sup> This may explain why, although HAP could increase bone mass by direct deposition, bone changes were not obvious until 12 weeks after administration.

Based on bone repair performance, 8 weeks was selected as the time point for implantation experiments. Osseointegration was assessed at 4 weeks after implantation to explore the early stability of the implant after CaP-PILP repair. In this study, osteoporotic bone repaired using CaP-PILP showed superior osseointegration. 3D reconstruction of Micro-CT was used to visualize the bone content around the implant. Further analysis of micro-CT data confirmed that CaP-PILP prosthetic bone showed early implant stabilization, similar to that of normal bone. The process of bone growth around an implant is similar to bone healing, and includes the three overlapping processes: inflammation, repair, and remodeling.<sup>8,70</sup> Insertion of the implant will cause bone damage and immediate inflammation, which continues for 3–4 days until the damage is mitigated.<sup>32,71</sup> Then, bone repair and remodeling commence. Bone with high fragility and poor biomechanical endurance will sustain more serious damage, which aggravates and prolongs inflammation,<sup>46,50</sup> and further deteriorates bone metabolism homeostasis;<sup>63</sup> this may have contributed to the poor osseointegration observed in OVX rats. Relative bone volume was slightly better in the HAP than the OVX group, but trabecular separation was surprisingly greater. This may be because the bone enhancement effect of HAP on osteoporotic bone was primarily mediated by direct deposition.<sup>72</sup> In the HAP group, collagen fibers remained in state of low mineralization, indicating that micromechanical parameters had not recovered. Furthermore, large amounts of HAP were recognized as foreign, which stimulated more active bone resorption.<sup>32,64</sup> CaP-PILP was designed and developed based on the biomimetic mineralization theory, and not only improved bone density but also enhanced bone strength characteristics by promoting intrafibrillar remineralization. After repairment, the bone is closer to normal bone in structure and function. Overall, CaP-PILP showed good osseointegration ability, similar to that of normal bone in the early stage of implant placement.

CaP-PILP shows notable advantages in bone repair and provides excellent support for the implant's early stability. Due to the difficulty of preparation, the previous research on ACP rarely involved ultra-small particle size. Although the advantages of mineralization in collagen are recognized, in practical applications, large particle size ACP is usually used as a reservoir of calcium and phosphorus ions.<sup>73</sup> In this study, we focused on the mineralization of collagen guided by ultra-small particle size ACP, which was rarely used in biomedical bone engineering. In vitro collagen fiber remineralization experiments showed that CaP-PILP could promote approximately 95% intrafibrillar mineralization.<sup>37</sup> Further, in vivo experiments showed that the fluidity of CaP-PILP allowed it to act directly in the surgical area by means of minimally invasive injection. The results demonstrated that CaP-PILP could significantly increase bone mineral density and biomechanical properties in an osteoporotic rat model to natural bone levels with a single dose of injection, which were helpful for implant fixation.

Natural bone provides inspiration for the development of new biomaterials used in bone repair and regeneration. Although CaP-PILP shows excellent application prospects, it also has several limitations to the present study. CaP-PILP is insufficient to provide the mineral mass required for rebuilding a healthy and suitable implant environment. Furthermore, ACP is extremely unstable, which provides a huge challenge for clinical application. Our future studies need to improve the properties of CaP-PILP for clinical application.

## Conclusion

In this study, we synthesized CaP-PILP, containing a high concentration of 1 nm ACP and confirmed that it could enhance the stability of early implant osseointegration in ovariectomized rats. CaP-PILP treatment transforms the structural and mechanical properties of osteoporotic bone. The use of bionic methods to develop biomaterials has gained increasing recognition. Our data provide new approaches for improving implant osseointegration in osteoporotic bone.

## Declaration

We have a cooperation with Zhejiang Chinese Medicine University Laboratory Animal Research Center, and we offer the project funding for the study. This center can provide animals and experimental equipment. Importantly, bone evaluation can be provided. Therefore, the animal experiment in this study was completed at this center.

## Acknowledgments

This research was supported by the Nation Key R&D program of China (2018YFC1105101) and the National Natural Science Foundation of China (81801024). The authors wish to thank Zheng Yuanna of Zhejiang Chinese Medicine University for their contributions. Zhou Yanyan and Hu Zihé should be considered joint first author.

## Disclosure

The authors report no conflicts of interest in this work.

## References

- Zhao H, Huang Y, Zhang W, et al. Mussel-inspired peptide coatings on titanium implant to improve osseointegration in osteoporotic condition. *Acs Biomater Sci Eng.* 2018;4(7):2505–2515. doi:10.1021/acsbomaterials.8b00261
- Gallagher JC. Advances in osteoporosis from 1970 to 2018. *Menopause.* 2018;25(12):1403–1417. doi:10.1097/GME.0000000000001263
- Bihui B, Xingwen X, Dingpeng L, Wei X, Ning L, Px U. Epidemiological studies on osteoporosis in the past five years in China. *Chin J Osteoporos.* 2018;24(2):253–258.
- Temmerman A, Rasmusson L, Kübler A, Thor A, Quirynen M. An open, prospective, non-randomized, controlled, multicentre study to evaluate the clinical outcome of implant treatment in women over 60 years of age with osteoporosis/osteopenia: 1-year results. *Clin Oral Implan Res.* 2017;28(1):95–102. doi:10.1111/clr.12766
- Fu X, Chen J, Wu D, et al. Effects of ovariectomy on rat mandibular cortical bone: a study using Raman spectroscopy and multivariate analysis. *Anal Chem.* 2012;84(7):3318–3323. doi:10.1021/ac300046x
- Otomo Corgel J. Osteoporosis and osteopenia: implications for periodontal and implant therapy. *Periodontol 2000.* 2012;59(1):111–139. doi:10.1111/j.1600-0757.2011.00435.x
- Twardowski SE, Wactawski-Wende J. Relationship between periodontal disease, tooth loss, and osteoporosis. In: Dempster DW, Cauley JA, Bouxsein ML, Cosman F, editors. *Marcus and Feldman's Osteoporosis.* New York: Academic Press; 2002:1381–1394.
- Alsaadi G, Quirynen M, Komárek A, van Steenberghe D. Impact of local and systemic factors on the incidence of oral implant failures, up to abutment connection. *J Clin Periodontol.* 2007;34(7):610–617. doi:10.1111/j.1600-051X.2007.01077.x
- Temmerman A, Rasmusson L, Kübler A, Thor A, Merheb J, Quirynen M. A prospective, controlled, multicenter study to evaluate the clinical outcome of implant treatment in women with osteoporosis/osteopenia: 5-year results. *J Dent Res.* 2019;98(1):84–90. doi:10.1177/0022034518798804
- Dreyer H, Grischke J, Tiede C, et al. Epidemiology and risk factors of peri-implantitis: a systematic review. *J Periodontol Res.* 2018;53(5):657–681. doi:10.1111/jre.12562
- Wagner F, Schuder K, Hof M, Heuberger S, Seemann R, Dvorak G. Does osteoporosis influence the marginal peri-implant bone level in female patients? A cross-sectional study in a matched collective. *Clin Implant Dent R.* 2017;19(4):616–623. doi:10.1111/cid.12493
- Ross RD, Hamilton JL, Wilson BM, Sumner DR, Viridi AS. Pharmacologic augmentation of implant fixation in osteopenic bone. *Curr Osteoporos Rep.* 2014;12(1):55–64. doi:10.1007/s11914-013-0182-z
- Zhao B, Li X, Xu H, Jiang Y, Wang D, Liu R. Influence of simvastatin-strontium-hydroxyapatite coated implant formed by micro-arc oxidation and immersion method on osteointegration in osteoporotic rabbits. *Int J Nanomed.* 2020;15:1797–1807. doi:10.2147/IJN.S244815

14. Meng X, Zhang J, Chen J, et al. KR-12 coating of polyether ether ketone (PEEK) surface via polydopamine improves osteointegration and antibacterial activity in vivo. *J Mater Chem B*. 2020;8(44):10190–10204. doi:10.1039/D0TB01899F
15. Chen Y, Lee K, Kawazoe N, Yang Y, Chen G. PLGA-collagen-ECM hybrid scaffolds functionalized with biomimetic extracellular matrices secreted by mesenchymal stem cells during stepwise osteogenesis-co-adipogenesis. *J Mater Chem B*. 2019;7(45):7195–7206. doi:10.1039/C9TB01959F
16. Merheb J, Temmerman A, Rasmusson L, Kübler A, Thor A, Quirynen M. Influence of skeletal and local bone density on dental implant stability in patients with osteoporosis. *Clin Implant Dent R*. 2016;18(2):253–260. doi:10.1111/cid.12290
17. Trullenque-Eriksson A, Guisado-Moya B. Retrospective long-term evaluation of dental implants in totally and partially edentulous patients. Part I. *Implant Dent*. 2014;23(6):732–737.
18. Wei H, Xu Y, Wang Y, et al. Identification of fibroblast activation protein as an osteogenic suppressor and anti-osteoporosis drug target. *Cell Rep*. 2020;33(2):108252. doi:10.1016/j.celrep.2020.108252
19. Harmankaya N, Karlsson J, Palmquist A, et al. Raloxifene and alendronate containing thin mesoporous titanium oxide films improve implant fixation to bone. *Acta Biomater*. 2013;9(6):7064–7073. doi:10.1016/j.actbio.2013.02.040
20. Li G, Zhang L, Wang L, et al. Dual modulation of bone formation and resorption with zoledronic acid-loaded biodegradable magnesium alloy implants improves osteoporotic fracture healing: an in vitro and in vivo study. *Acta Biomater*. 2017;65:486–500. doi:10.1016/j.actbio.2017.10.033
21. Alghamdi HS, Junker R, Bronkhorst EM, Jansen JA. Bone regeneration related to calcium phosphate-coated implants in osteoporotic animal models: a meta-analysis. *Tissue Eng Part B Rev*. 2012;18(5):383–395. doi:10.1089/ten.teb.2012.0130
22. Alghamdi HS, Cuijpers VMJI, Wolke JGC, van den Beucken JJJP, Jansen JA. Calcium-phosphate-coated oral implants promote osseointegration in osteoporosis. *J Dent Res*. 2013;92(11):982–988. doi:10.1177/0022034513505769
23. Ding X, Yang L, Hu Y. Effect of local application of bisphosphonates on improving peri-implant osseointegration in type-2 diabetic osteoporosis. *Am J Transl Res*. 2019;11(9):5417–5437.
24. Wang P, Zhao L, Liu J, Weir MD, Zhou X, Xu HHK. Bone tissue engineering via nanostructured calcium phosphate biomaterials and stem cells. *Bone Res*. 2014;2(1). doi:10.1038/boneres.2014.17
25. de Melo Pereira D, Habibovic P. Biomimetic-Inspired material design for bone regeneration. *Adv Healthc Mater*. 2018;7(22):1800700. doi:10.1002/adhm.201800700
26. Al B, Tm W, Rd B. Perspective collagen and bone strength. *J Bone Miner Res*. 1999;14(3):330–335. doi:10.1359/jbmr.1999.14.3.330
27. Mosekilde L, Ebbesen EN, Tornvig L, Thomsen JS. Trabecular bone structure and strength - remodelling and repair. *J Musculoskelet Neuronal Interact*. 2000;1(1):25–30.
28. Ozasa R, Ishimoto T, Miyabe S, et al. Osteoporosis Changes Collagen/Apatite Orientation and Young's Modulus in Vertebral Cortical Bone of Rat. *Calcified Tissue Int*. 2019;104(4):449–460. doi:10.1007/s00223-018-0508-z
29. Gröniger O, Hess S, Mohn D, et al. Directing stem cell commitment by amorphous calcium phosphate nanoparticles incorporated in PLGA: relevance of the free calcium ion concentration. *Int J Mol Sci*. 2020;21(7):2627. doi:10.3390/ijms21072627
30. Zhang X, Wang Y, Manh N, Wang H, Zhong X, Li C. Synergistic intrafibrillar/extrafibrillar mineralization of collagen scaffolds based on a biomimetic strategy to promote the regeneration of bone defects. *Int J Nanomed*. 2016;2053. doi:10.2147/IJN.S102844
31. Eliaz N, Metoki N. Calcium phosphate bioceramics: a review of their history, structure, properties, coating technologies and biomedical applications. *Materials*. 2017;10(4):334.
32. Cantaert B, Beniash E, Meldrum FC. Nanoscale confinement controls the crystallization of calcium phosphate: relevance to bone formation. *Chem Eur J*. 2013;19(44):14918–14924. doi:10.1002/chem.201302835
33. Maté Sánchez De Val JE, Calvo-Guirado JL, Gómez-Moreno G, Pérez-Albacete Martínez C, Mazón P, De Aza PN. Influence of hydroxyapatite granule size, porosity, and crystallinity on tissue reaction in vivo. Part A: synthesis, characterization of the materials, and SEM analysis. *Clin Oral Implan Res*. 2016;27(11):1331–1338. doi:10.1111/clr.12722
34. Gelli R, Ridi F, Baglioni P. The importance of being amorphous: calcium and magnesium phosphates in the human body. *Adv Colloid Interfac*. 2019;269:219–235.
35. Yang H, Niu L, Sun J, et al. Biodegradable mesoporous delivery system for biomineralization precursors. *Int J Nanomed*. 2017;12:839–854.
36. Zhao C, Qazvini NT, Sadati M, et al. A pH-triggered, self-assembled, and bioprintable hybrid hydrogel scaffold for mesenchymal stem cell based bone tissue engineering. *ACS Appl Mater Inter*. 2019;11(9):8749–8762. doi:10.1021/acsami.8b19094
37. Yao S, Lin X, Xu Y, et al. Osteoporotic bone recovery by a highly bone-inductive calcium phosphate polymer-induced liquid-precursor. *Adv Sci*. 2019;6(19):1900683. doi:10.1002/adv.201900683
38. Yao S, Xu Y, Zhou Y, et al. Calcium phosphate nanocluster-loaded injectable hydrogel for bone regeneration. *ACS Applied Bio Materials*. 2019;2(10):4408–4417. doi:10.1021/acsabm.9b00270
39. Luo E, Hu J, Bao C, et al. Sustained release of adiponectin improves osteogenesis around hydroxyapatite implants by suppressing osteoclast activity in ovariectomized rabbits. *Acta Biomater*. 2012;8(2):734–743. doi:10.1016/j.actbio.2011.10.029
40. Gomes-Ferreira PHS, de Oliveira D, Frigério PB, de Souza Batista FR, Grandfield K, Okamoto R. Teriparatide improves micro-architectural characteristics of peri-implant bone in orchietomized rats. *Osteoporosis Int*. 2020;31(9):1807–1815. doi:10.1007/s00198-020-05431-y
41. Dempster DW, Compston JE, Drezner MK, et al. Standardized nomenclature, symbols, and units for bone histomorphometry: a 2012 update of the report of the ASBMR Histomorphometry Nomenclature Committee. *J Bone Miner Res*. 2013;28(1):1–16. doi:10.1002/jbmr.1805
42. Clynes MA, Harvey NC, Curtis EM, Fuggle NR, Dennison EM, Cooper C. The epidemiology of osteoporosis. *Brit Med Bull*. 2020;133(1):105–117.
43. Zhang J, Dennison E, Prieto-Alhambra D. Osteoporosis epidemiology using international cohorts. *Curr Opin Rheumatol*. 2020;32(4):387–393. doi:10.1097/BOR.0000000000000722
44. Du Z, Xiao Y, Hashimi S, Hamlet SM, Ivanovski S. The effects of implant topography on osseointegration under estrogen deficiency induced osteoporotic conditions: histomorphometric, transcriptional and ultrastructural analysis. *Acta Biomater*. 2016;15(42):351–363. doi:10.1016/j.actbio.2016.06.035
45. Young MF. Bone matrix proteins: their function, regulation, and relationship to osteoporosis. *Osteoporosis Int*. 2003;14(S3):35–42. doi:10.1007/s00198-002-1342-7
46. Seeman E, Delmas PD. Bone quality—the material and structural basis of bone strength and fragility. *N Engl J Med*. 2006;354(21):2250–2261. doi:10.1056/NEJMra053077
47. Barrère F, van Blitterswijk CA, de Groot K. Bone regeneration: molecular and cellular interactions with calcium phosphate ceramics. *Int J Nanomed*. 2006;1(3):317–332.
48. Norio Matsushima KH. Age changes in the crystallinity of bone mineral. *Biochim Biophys Acta Gen Subj*. 1989;992(2):155–159. doi:10.1016/0304-4165(89)90004-4
49. Alghamdi HS, Jansen JA. Bone regeneration associated with non-therapeutic and therapeutic surface coatings for dental implants in osteoporosis. *Tissue Eng Part B Rev*. 2013;19(3):233–253. doi:10.1089/ten.teb.2012.0400

50. Beppu K, Kido H, Watazu A, Teraoka K, Matsuura M. Peri-implant bone density in senile osteoporosis—changes from implant placement to osseointegration. *Clin Implant Dent R*. 2013;15(2):217–226. doi:10.1111/j.1708-8208.2011.00350.x
51. Dayer R, Badoud I, Rizzoli R, Ammann P. Defective implant osseointegration under protein undernutrition: prevention by PTH or pamidronate. *J Bone Miner Res*. 2007;22(10):1526–1533. doi:10.1359/jbmr.070610
52. Almagro MI, Roman-Blas JA, Bellido M, Castañeda S, Cortez R, Herrero-Beaumont G. PTH [1-34] enhances bone response around titanium implants in a rabbit model of osteoporosis. *Clin Oral Implan Res*. 2012;24(9):1027–1034.
53. Mu C, Hu Y, Huang L, et al. Sustained raloxifene release from hyaluronan-alendronate functionalized titanium nanotube arrays capable of enhancing osseointegration in osteoporotic rabbits. *Mat Sci Eng C-Mater*. 2017;1(82):345–353.
54. Basudan AM, Shaheen MY, de Vries RB, van den Beucken JJP, Jansen JA, Alghamdi HS. Antiosteoporotic drugs to promote bone regeneration related to titanium implants: a systematic review and meta-analysis. *Tissue Eng Part B Rev*. 2019;25(2):89–99. doi:10.1089/ten.teb.2018.0120
55. Zhou W, Liu Y, Shen J, et al. Melatonin increases bone mass around the prostheses of OVX rats by ameliorating mitochondrial oxidative stress via the SIRT3/SOD2 signaling pathway. *Oxid Med Cell Longev*. 2019;2019:1–16.
56. Tao Z, Zhou W, He X, et al. A comparative study of zinc, magnesium, strontium-incorporated hydroxyapatite-coated titanium implants for osseointegration of osteopenic rats. *Mat Sci Eng C-Mater*. 2016;62:226–232. doi:10.1016/j.msec.2016.01.034
57. Wang L, Nancollas GH. Dynamics of Biomineralization and Biodemineralization. *Met Ions Life Sci*. 2008;4:413–456.
58. Wang L, Nancollas GH. Pathways to biomineralization and biodemineralization of calcium phosphates: the thermodynamic and kinetic controls. *Dalton T*. 2009;1(15):2665. doi:10.1039/b815887h
59. Combes C, Rey C. Amorphous calcium phosphates: synthesis, properties and uses in biomaterials. *Acta Biomater*. 2010;6(9):3362–3378. doi:10.1016/j.actbio.2010.02.017
60. Jiang S, Jin W, Wang Y, Pan H, Sun Z, Tang R. Effect of the aggregation state of amorphous calcium phosphate on hydroxyapatite nucleation kinetics. *Rsc Adv*. 2017;7(41):25497–25503. doi:10.1039/C7RA02208E
61. Liu Y, Zhu Z, Pei X, et al. ZIF-8-modified multifunctional bone-adhesive hydrogels promoting angiogenesis and osteogenesis for bone regeneration. *Acs Appl Mater Inter*. 2020;12(33):36978–36995. doi:10.1021/acsami.0c12090
62. Alghamdi HS, Bosco R, Both SK, et al. Synergistic effects of bisphosphonate and calcium phosphate nanoparticles on peri-implant bone responses in osteoporotic rats. *Biomaterials*. 2014;35(21):5482–5490. doi:10.1016/j.biomaterials.2014.03.069
63. Li A, Xie J, Li J. Recent advances in functional nanostructured materials for bone-related diseases. *J Mater Chem B*. 2019;7(4):509–527. doi:10.1039/C8TB02812E
64. Uskoković V, Janković-častvan I, Wu VM. Bone mineral crystallinity governs the orchestration of ossification and resorption during bone remodeling. *Acs Biomater Sci Eng*. 2019;5(7):3483–3498. doi:10.1021/acsbomaterials.9b00255
65. Chen X, Bai J, Yuan S, et al. Calcium phosphate nanoparticles are associated with inorganic phosphate-induced osteogenic differentiation of rat bone marrow stromal cells. *Chem-Biol Interact*. 2015;238:111–117. doi:10.1016/j.cbi.2015.06.027
66. Li X, van Blitterswijk CA, Feng Q, Cui F, Watari F. The effect of calcium phosphate microstructure on bone-related cells in vitro. *Biomaterials*. 2008;29(23):3306–3316. doi:10.1016/j.biomaterials.2008.04.039
67. Wu VM, Uskoković V. Is there a relationship between solubility and resorbability of different calcium phosphate phases in vitro? *Biochim Biophys Acta Gen Subj*. 2016;1860(10):2157–2168. doi:10.1016/j.bbagen.2016.05.022
68. Dorozhkin S. Nanodimensional and nanocrystalline apatites and other calcium orthophosphates in biomedical engineering, biology and medicine. *Materials*. 2009;2(4):1975–2045.
69. Allegrini S, Da Silva AC, Tsujita M, Salles MB, Gehrke SA, Braga FJC. Amorphous calcium phosphate (ACP) in tissue repair process. *Microsc Res Techniq*. 2018;81(6):579–589. doi:10.1002/jemt.23013
70. Kyllönen L, Este D, Alini M, Eglin D. Local drug delivery for enhancing fracture healing in osteoporotic bone. *Acta Biomater*. 2015;11:412–434.
71. Przekora A. Current trends in fabrication of biomaterials for bone and cartilage regeneration: materials modifications and biophysical stimulations. *Int J Mol Sci*. 2019;20(2):435. doi:10.3390/ijms20020435
72. Betty León JAJ. *Thin Calcium Phosphate Coatings for Medical Implants*. Springer; 2009.
73. Yokota S, Nishiwaki N, Ueda K, Narushima T, Kawamura H, Takahashi T. Evaluation of thin amorphous calcium phosphate coatings on titanium dental implants deposited using magnetron sputtering. *Implant Dent*. 2014;23(3):343–350. doi:10.1097/ID.000000000000098

## International Journal of Nanomedicine

### Publish your work in this journal

The International Journal of Nanomedicine is an international, peer-reviewed journal focusing on the application of nanotechnology in diagnostics, therapeutics, and drug delivery systems throughout the biomedical field. This journal is indexed on PubMed Central, MedLine, CAS, SciSearch®, Current Contents®/Clinical Medicine,

Submit your manuscript here: <https://www.dovepress.com/international-journal-of-nanomedicine-journal>

Journal Citation Reports/Science Edition, EMBase, Scopus and the Elsevier Bibliographic databases. The manuscript management system is completely online and includes a very quick and fair peer-review system, which is all easy to use. Visit <http://www.dovepress.com/testimonials.php> to read real quotes from published authors.